

1 Possible threshold controls on sediment grain properties of
2 Peruvian coastal river basins

3

4 **Camille Litty¹, Fritz Schlunegger¹, Willem Viveen²**

5

6 ¹ *Institute of Geological Sciences, University of Bern, Baltzerstrasse 1+3, CH- 3012 Bern.*

7 ² *Grupo de investigación en geología sedimentaria, Pontificia Universidad Católica del Perú,*
8 *Av. Universitaria 1801, San Miguel, Lima, Perú.*

9

10 **ABSTRACT**

11 Twenty-one coastal rivers located along the entire western Peruvian margin were analyzed to
12 determine possible controls on sediment grain properties. This represents one of the largest grain
13 size dataset that has been collected over a large area. Modern gravel beds were sampled along a
14 north-south transect on the western side of the Peruvian Andes where the rivers cross the tip of
15 the mountain range, and at each site the long *a*-axis and the intermediate *b*-axis of about 500
16 pebbles were measured. Morphometric properties of each drainage basin, sediment and water
17 discharge together with flow shear stresses were determined and compared against measured
18 grain properties. Grain size data show that the values for the D_{50} are nearly constant and range
19 between 2-3 cm, while the values of the D_{96} range between 6 and 12 cm. The ratios between the
20 intermediate and the long axis range from 0.67 to 0.74. Linear correlations between all grain size
21 percentiles and water shear stresses, mean basin denudation rates, mean basin slopes and basin
22 sizes are small to non-existent. However exceptionally large D_{50} values of 4-6 cm were measured
23 for basins situated between 11-12°S and 16-17°S latitude where hillslope gradients are steeper

24 than on the average or where mean annual stream flows exceed the average values of the western
25 Peruvian streams by a factor of 2. We suggest that the generally uniform grain size pattern has
26 been perturbed where either mean basin slopes, or water fluxes exceed threshold conditions.

27

28 **1. INTRODUCTION**

29 The size and shape of gravels bear crucial information about (i) the transport dynamics of
30 mountain rivers (Hjulström, 1935; Shields, 1936; Blissenbach, 1952; Koiter et al., 2013;
31 Whittaker et al., 2007; Duller et al., 2012; Attal et al., 2015), (ii) the mechanisms of sediment
32 supply and provenance (Parker, 1991; Paola et al., 1992a, b; Attal and Lavé, 2006), and (iii)
33 environmental conditions such as uplift and precipitation (Heller and Paola, 1992; Robinson and
34 Slingerland, 1998; Foreman et al., 2012; Allen et al., 2013; Foreman, 2014). The mechanisms by
35 which grain size and shape change from source to sink have often been studied with flume
36 experiments (e.g. McLaren and Bowles, 1985; Lisle et al., 1993) and numerical models (Hoey
37 and Ferguson, 1994). These studies have mainly been directed towards exploring the controls on
38 the downstream reduction in grain size of gravel beds (Schumm and Stevens, 1973; Hoey and
39 Fergusson, 1994; Surian, 2002; Fedele and Paola, 2007; Allen et al., 2016). In addition, it has
40 been proposed that the grain size distribution particularly of mountainous rivers mainly depends
41 on: (i) tectonic uplift resulting in steepening of the entire landscape (Dadson et al., 2003;
42 Wittmann et al., 2007; Ouimet et al., 2009), (ii) earthquakes and seismicity causing the release of
43 large volumes of landslides (Dadson et al., 2003; McPhillips et al., 2014); (iii) precipitation rates
44 and patterns controlling river discharge and shear stresses (D'Arcy et al., 2017; Litty et al.,
45 2017); and (iv) bedrock lithology where low erodibility lithologies are sources of larger volumes
46 of material (Korup and Schlunegger, 2009, Allen et al., 2015). Accordingly, the sediment caliber

47 in these rivers could either reflect the nature of erosional processes in the headwaters and
48 conditions thereof (such as lithology, slope angles, seismicity releasing landslides), which then
49 correspond to supply-limited conditions. Alternatively, if enough material is supplied to the
50 streams, then the grain size pattern mainly depends on the runoff and related shear stresses in
51 these rivers, which in turn correspond to transport-limited conditions.

52 The western margin of the Peruvian Andes represents a prime example where these mechanisms
53 and related controls on the grain size distribution of river sediments can be explored. In
54 particular, this mountain belt experiences intense and frequent earthquakes (Nocquet et al., 2014)
55 in response to subduction of the oceanic Nazca plate beneath the continental South American
56 plate at least since late Jurassic times (Isacks, 1988). Therefore, it is not surprising that erosion
57 and the transfer of material from the hillslopes to the rivers has been considered to strongly
58 depend on the occurrence of earthquakes (McPhillips et al., 2014). On the other hand, it has also
59 been proposed that denudation in this part of the Andes is controlled by distinct precipitation rate
60 gradients. These inferences have been made based on concentrations of in-situ cosmogenic ^{10}Be
61 measured in river-born quartz (Abbühl et al., 2011; Carretier et al., 2015; Reber et al., 2017), and
62 on morphometric analyses of the western Andean landscape (Montgomery et al., 2001).
63 Accordingly, erosion along the western Peruvian Andes has been related to either the occurrence
64 of earthquakes and thus to tectonic processes (McPhillips et al., 2014) or rainfall rates (Abbühl et
65 al., 2011; Carretier et al., 2015) and to the stream's mean annual runoff and thus to climatic
66 processes (Reber et al., 2017). Therefore, we hypothesize that hillslope erosion paired with the
67 streams runoff are likely to have a measurable impact on the grain size pattern in the Peruvian
68 streams.

69 Here we present data on sediment grain properties from rivers situated on the western margin of
70 the Peruvian Andes (Figure 1A) in order to elucidate the possible effects of intrinsic factors such
71 as morphometric properties of the drainage basins (mean slope, drainage area, stream lengths),
72 and extrinsic properties (runoff and seismic activity) on sediment grain properties. To this extent,
73 we collected grain size data from gravel bars of each stream along the entire western Andean
74 margin of Peru that are derived from 21, over 700-km²-large basins. Sampling sites were situated
75 at the outlets of valleys close to the Pacific Coast. This represents one of the largest grain size
76 dataset that has ever been collected over areas which have experienced different tectonic and
77 climatic conditions.

78

79 *1.1 Geologic and tectonic setting*

80 The study area is located at the transition from the Peruvian Andes to the coastal lowlands along
81 a transect from the cities of Trujillo in the north (8°S) to Tacna in the south (18°S). In northern
82 and central Peru, a flat, up-to 100 km wide, broad coastal forearc plain with Paleogene-Neogene
83 and Quaternary sediments connects to the western Cordillera. This part of the western Cordillera
84 consists of Cretaceous to late Miocene plutons of various compositions (diorite, but also tonalite,
85 granite and granodiorite) that crop out over an almost continuous, 1600-km long arc that is
86 referred to as the Coastal Batholith (e.g. Atherton, 1984; Mukasa, 1986; Haederle and Atherton,
87 2002; Figure 1B). In southern Peru, the coastal plain gives way to the Coastal Cordillera that
88 extends far into Chile. The western Cordillera comprises the central volcanic arc region of the
89 Peruvian Andes with altitudes of up to 6768 m.a.s.l., where currently active volcanoes south of
90 14°S of latitude are related to a steep slab subduction. On the other hand, Cenozoic volcanoes in

91 the central and northern Peruvian arc have been extinct since c. 11 Ma due to a flat slab
92 subduction, which inhibited magma upwelling from the asthenosphere (Ramos, 2010).

93 The bedrock of the Western Cordillera is dominated by Paleogene, Neogene and Quaternary
94 volcanic rocks (mainly andesitic or dacitic tuffs, and ignimbrites) originating from distinct
95 phases of Cenozoic volcanic activity (Vidal, 1993). These rocks rest on Mesozoic and Early
96 Paleogene sedimentary rocks (Figure 1B).

97 The tectonic conditions of the western Andes are characterized by strong N-S gradients in
98 Quaternary uplift, seismicity and long-term subduction processes, which in turn seem controlled
99 by a plethora of tectonic processes. The northern segment of the coastal Peruvian margin (i.e. to
100 the north of 13°S latitude), hosts a coastal plain that shows little evidence for uplift, and the
101 Nazca plate subducts at a low angle. Also in this region, the occurrence of large historical
102 earthquakes at least along the coastal segment has been much less (Figure 2c). Only in
103 northernmost Peru (4° to 6° S latitude) uplift of the coastal area is associated with subduction
104 induced earthquakes (Bourgeois et al., 2007). Further south, the Cordillera Blanca area (around
105 12° S latitude) may have been uplifted due to upwelling of magma (McNulty and Farber, 2002).
106 In particular, the coastal segment south of 13°S hosts raised Quaternary marine terraces (Regard
107 et al., 2010), suggesting the occurrence of surface uplift at least during Quaternary times. Since
108 the number and altitude of the terraces increases closer to the area where currently the Nazca
109 ridge subducts, uplift of the coastal area in a radius of approximately 200 km around the ridge
110 (roughly 12° to 14° S latitude) is attributed to ridge subduction (Sébrier et al., 1988; Macharé
111 and Ortlieb, 1992). Between 15° and 18° S latitude, uplift is associated with bending of the
112 Bolivian orocline (Noury et al., 2016). The area south of 12° S latitude is also the segment of the
113 Andes where the number of earthquakes with magnitudes > 4 has been larger relative to the

114 segment farther north (Figures 1 and 2c). In contrast, the northern segment of the coastal
115 Peruvian margin (i.e., to the north of 13°S latitude), hosts a coastal plain that has been subsiding
116 and the Nazca plate subducts at a low angle. Also in this region, the frequency of large historical
117 earthquakes at least along the coastal segment has been much less (Figure 2c)

118

119 *1.2 Morphological setting*

120 The local relief along the western Cordillera has been formed by deeply incising rivers that flow
121 perpendicular to the strike of the Andes (Schildgen et al., 2007). The morphology of the
122 longitudinal stream profiles is characterized by two segments separated by a distinct knickzone
123 (Trauerstein et al., 2013). These geomorphic features have formed through headward retreat in
124 response to a phase of enhanced surface uplift during the late Miocene (e.g., Schildgen et al.,
125 2007). Upstream of these knickzones, the streams are mainly underlain by Cenozoic
126 volcanoclastic rocks, while farther downstream incision has disclosed the Coastal Batholith and
127 older meta-sedimentary units (Trauerstein et al. 2013). The upstream edges of these knickzones
128 also delineate the upper boundary of the major sediment sources (Litty et al., 2017). Little to
129 nearly zero clastic material is derived from the headwater reaches on the Altiplano, where the flat
130 landscape is experiencing nearly zero erosion, as ^{10}Be -based denudation rate estimates (Abbühl
131 et al., 2011) and provenance tracing have shown (Litty et al., 2017).

132 The pattern of mean slopes per drainage basin reveals a distinct S-N trend (Table 1). The
133 corresponding values increase from 20° to 25° going from 6°S to 10°S latitude (where they reach
134 maximum values between 0.4 to 0.45 m/m) after which they decrease by nearly 50% to values
135 ranging between 10° and 15° further north. These relationships have not been explored yet, but
136 most likely reflect the extent to which streams have crossed the western escarpment and sourced

137 their waters in the relatively flat plateau of the Puna region. Indeed, most of the western Peruvian
138 streams have their water sources on this flat area and then cross the western escarpment, which
139 yields relatively low mean basin slopes particularly for basins south of 12°S. On the other hand,
140 the basins around 11°-12°S latitudes (which are characterized by the steep slopes) have their
141 sources in the relatively steep Cordillera Negra (Figure 1A), which is a relatively dry mountain
142 range situated on the steep escarpment. Along these latitudes, the high Andes are constituted by
143 the high and heavily glaciated Cordillera Blanca situated farther to the east (Figure 1A). This
144 mountain range is drained by the Rio Santa, which flows parallel to the Andes strike, and then
145 crosses the Cordillera Negra at a right angle (Figure 1A).

146

147 *1.2 Climatic setting and stream runoff*

148 The Peruvian western margin shows an E-W contrasting precipitation pattern with high annual
149 precipitation rates up to 800 mm on the Altiplano and c. 0 mm per year on the coast ((Huffman et
150 al., 2007; Figure 1C). This precipitation gradient in the western Andes is related to the position
151 of the Intertropical Convergence Zone (ITCZ, inset of Figure 1C) associated with an orographic
152 effect on the eastern side of the Andes (Bookhagen and Strecker, 2008). During austral summer
153 (January) the center of the ITCZ is located farther south, transferring the moisture from the
154 Amazon tropical basin to the Altiplano (Garreaud et al., 2009) and leading to a wet climate on
155 the Altiplano with high precipitation rates. During austral winter, the Altiplano is under the
156 influence of dry air masses from the subsiding branch of the Hadley cell that result in a more
157 equatorial position of the ITCZ and in a dry persistent westerly wind with almost no precipitation
158 on the Altiplano. Additionally, the Andes form an orogenic barrier preventing Atlantic winds and
159 moisture from reaching the coast. In addition, every 2 to 10 years, near to the Equator, the

160 Pacific coast is subjected to strong precipitation resulting in high flood variability, related to the
161 El Niño weather phenomenon (DeVries, 1987).
162 Mean annual discharge of streams along the western Peruvian margin has been reported by
163 Reber et al. (2017). These authors calculated mean annual discharge values using the TRMM-
164 V6.3B43.2 precipitation database by Huffman et al. (2007) as a basis. Reber et al. (2017, see
165 their Table 3) and corrected the theoretical values for water losses due to evaporation and
166 irrigation using the gauging record of a minimum of 12 basins situated close to the Pacific ocean.
167 For these areas hydrological data has been reported by the Sistema Nacional de Información de
168 Recursos Hídricos (SNIRH). The hydrological data thus cover a time span of c. 12 years. The
169 results show a pattern where mean annual runoff of these streams ranges between c. 10-40 m³/s.
170 Rivers where mean annual runoff values are nearly 80 m³/s comprise the Rio Santa at c. 9°S
171 latitude (Figure 1A), which derives its water from glaciers in the Cordillera Blanca. Two other
172 streams with high discharge values are situated at 16°-17°S (Rio Ocoña and Rio Camaña, Figure
173 1A) where the corresponding headwaters spread over a relatively large area across the Altiplano,
174 thereby collecting more rain than the other basins.

175

176 2. SITE SELECTION AND METHODS

177 Sampling sites are situated in the main river valleys in the western Cordillera between 8°S and
178 18°S latitude just before it gives way to the coastal margin. 21 river basins larger than 700 km²
179 were selected. We selected the downstream end of these rivers for simplicity and because this
180 yields comparable conditions as the base level is the same for all streams. Sampling sites are all
181 accessible along the Pan-American Highway (see Table 1 for the coordinates of the sampling
182 sites). Additionally, the Majes basin (marked with red color on Figure 1A) has been sampled at

183 five sites from upstream to downstream to explore the effects related to the sediment transport
184 processes for a section across the mountain belt, but along the stream (Figure 3; Table 2). The
185 Majes basin has been chosen because of its easy accessibility in the upstream direction and
186 because the morphology of this basin has been analyzed in a previous study (Steffen et al.,
187 2010).

188 At each sampling site, we randomly selected five longitudinal bars where we collected our grain
189 size dataset. It has been shown that using a standard frame with fixed dimensions to assist gravel
190 sampling reduces user-biased selections of gravels (Marcus et al., 1995; Bunte and Abt, 2001a).
191 In order to reduce this bias, we substituted the frame by shooting an equal number of photos at a
192 fixed distance (c. 1 m) from the ground surface at each longitudinal bar. Ten photos were taken
193 from an approximately 10 m²-large area to take potential spatial variabilities among the gravel
194 bars into account. From those photos, the intermediate *b*-axes and the ratio of the *b*-axes and the
195 long *a*-axis of around 500 randomly chosen pebbles were manually measured (Bunte and Abt,
196 2001b) and processed using the software program ImageJ (Rasband, 1997). Our sample
197 population exceeds the minimum number of samples needed for statistically reliable estimations
198 of grain size distributions in gravel bars (Howard, 1993; Rice and Church, 1998).

199 The pebbles were characterized on the basis of their median (D_{50}), the D_{84} and the coarse (D_{96})
200 fractions. This means that 50%, 84% and 96% of the sampled fraction is finer grained than the
201 50th, 84th and 96th percentiles of the samples. On a gravel bar, pebbles tend to lie with their short
202 axis perpendicular to the surface, thus exposing their section that contains the *a*- and *b*-axes
203 (Bunte and Abt, 2001b). However, the principal limitation is the inability to accurately measure
204 the fine particles < 3 mm (see also Whittaker et al., 2010). While we cannot resolve this problem
205 with the techniques available, we do not expect that this adds a substantial bias in the grain size

206 distributions reported here as their relative contributions to the point count results are minor (i.e.
 207 < 5%, based on visual inspection of the digital images).

208 Catchment-scale morphometric parameters and characteristics, including drainage area, mean
 209 slope angle for each catchment, slope angle of the stream channel at the sampling site and
 210 distances from the sampling sites to the upper edge of the Western Escarpment were extracted
 211 from the 90-m-resolution digital elevation model (DEM) Shuttle Radar Topography Mission
 212 (SRTM; Reuter et al., 2007).

213 Because grain size pattern largely depends on water shear stresses, we explored the possible
 214 correlations between water shear stresses and grain size distribution. We thus computed water
 215 shear stresses τ following Hancock and Anderson (2002) and Litty et al. (2016), where:

$$216 \quad \tau = 0.54\rho g \left(\frac{Q}{W}\right)^{0.55} S^{0.93} \quad (1).$$

217 Here, $\rho=1000 \text{ kg/m}^3$ is the water density, g the gravitational acceleration, Q (m^3/s) is the mean
 218 annual water discharge that we have taken from Reber et al. (2017), W (m) the channel width,
 219 and S (m/m) is the channel gradient. Stream channel widths with an estimated error of 2 m were
 220 measured on satellite images where available, and on photos taken during the field campaign.

221 We were also interested in exploring whether sediment flux has a measurable impact on the grain
 222 size pattern because higher denudation rates could be associated with the supply of more coarse-
 223 grained material to the trunk stream. This in turn could result in larger clasts in these streams and
 224 could potentially cause gravel fronts to shift towards more distal sites (Dingle et al., 2017),
 225 thereby coarsening the sediment caliber at our sampling sites. These basins have recently been
 226 analyzed for ^{10}Be -based catchment averaged denudation rates and mean annual water fluxes
 227 (please see Reber et al., 2017, and information presented above). This allows us to explore

228 whether sediment flux, which equals the product between ^{10}Be -based denudation rates and basin
229 size, has a measurable impact on the grain size pattern.

230 Possible covariations and correlations between grain size and/or morphometric parameters and
231 basin characteristics were evaluated using Pearson correlation coefficients, thus providing
232 corresponding r-values (Table 3). The r-values measure the linear correlations between variables.
233 The values range between +1 and -1, where +1 reflects a 100% positive linear correlation, 0
234 reflects no linear correlation, and -1 indicates a 100% negative linear correlation (Pearson,
235 1895). Threshold values of $> + 0.30$ and $< - 0.30$ were selected to assign positive and negative
236 correlations, respectively.

237

238 **3. RESULTS**

239 ***3.1 Grain size***

240 The results of the grain size measurements reveal a large variation of the *b*-axis. The D_{50} values
241 range from 1.3 cm to 5.5 cm (Figure 2h; Table 1). Likewise, D_{84} values vary between 3 cm and
242 10.5 cm. The sizes for the D_{96} reveal the largest spread, ranging from 6 cm to 31 cm. The ratio
243 between the *b*-axis and *a*-axis (sphericity ratio) is nearly constant and varies between 0.67 and
244 0.74 (Figure 2i). Note that between 15.6°S and 13.7°S , no gravel bars are encountered in the
245 rivers where they leave the mountain range, and only sand bars can be found. Therefore no
246 results are exhibited for these latitudes (Figure 2h and 2i).

247

248 ***3.2 The Majes basin***

249 The D_{50} percentile of the *b*-axis decreases from 6.2 cm to a value of 5.2 cm c. 80 km farther
250 downstream (Figures 3 and 4 and Table 2). Likewise, the D_{84} decreases from 19 cm to 8.7 cm,

251 and the D_{96} decreases from 31 cm to 11.6 cm (Figure 4). Geomorphologists widely accept the
252 notion that the downstream hydraulic geometry of alluvial channels reflects the decrease of
253 particle size within an equilibrated system involving stream flow, channel gradient, sediment
254 supply and transport (Hoey and Ferguson, 1994; Fedele and Paola, 2007; Attal and Lavé, 2009).
255 Sternberg (1875) formalized these relations and predicted an exponential decline in particle size
256 in gravel-bed rivers as a consequence of abrasion and selective transport where the gravel is
257 transported downstream. The relation follows the form: $D_x = D_0 e^{-\alpha x}$ (Sternberg, 1875). Here,
258 the gthree percentiles follow an exponential fining decrease with the exponent α ranging from
259 0.3 for the D_{96} to 0.1 for the D_{50} (Figure 4).

260

261 ***3.3 Correlations between grain sizes and morphometric properties***

262 Table 3 shows the Pearson correlation coefficients (r-value) between the grain sizes, the
263 morphometric parameters and the characteristics of the basins. As was expected, the D_{50} , D_{84} and
264 D_{96} all strongly correlate with each other ($0.73 < r\text{-value} < 0.93$), but the b/a ratios do not
265 correlate with any of the three percentiles ($-0.1 < r\text{-value} < 0.1$). Likewise, inter-correlation
266 relationships also exist among other variables such as catchment area, distance from the western
267 escarpment, sediment flux and water discharge (Table 3). The D_{50} values positively but weakly
268 correlate with the sizes of the catchment area (r-value = 0.31), the distances from the Western
269 Escarpment (r-value = 0.35), the mean annual shear stresses at the sampling site (r-value = 0.23),
270 the denudation rates (r-value = 0.34) and the sediment fluxes (r-value = 0.42; Table 3). The D_{84}
271 and the D_{96} values correlate positively with the mean annual shear stresses exerted by the water
272 flux with relative low r-value of 0.33 and 0.39 (Table 3).

273 At a broader scale, values of the D_{50} are nearly constant between 2 and 3 cm (Table 3). The
274 largest D_{50} with values of up to 6 cm are encountered in streams that are either sourced in the
275 Cordillera Negra where mean basin slope angles are larger than 20° , or in the Rio Ocoña and Rio
276 Camaña rivers located at 16° - 17° S, which have the largest mean annual discharge as they capture
277 their waters from a broad area on the Altiplano.

278 The ratio of the intermediate axis over the long axis negatively correlates with the distance from
279 the Western Escarpment (r -value = -0.33), albeit with a poor correlation, but a strong and
280 positive correlation is found with the mean slope angles of the basins (r -value = 0.63; Table 3).

281

282 **4. DISCUSSION**

283

284 4.1 SLOPE ANGLE CONTROLS ON SPHERICITY

285 The poor negative correlation of -0.33 between the sphericity of the pebbles and distance from
286 the escarpment edge (Table 3) prevents us from inferring a distinct control of this variable. On
287 the other hand, the positive Pearson correlation of 0.63 between the sphericity of the pebbles and
288 the mean basin slope is quite high (Table 3), thus pointing towards a significant control. This
289 suggests that basins with steeper slopes produce rounder pebbles. We do not consider that this
290 pattern is due to differences in exposed bedrock in the hinterland because the litho-tectonic
291 architecture is fairly constant along the entire Peruvian margin (Figure 1). We tentatively infer
292 that time scales of transport and evacuation of material are likely to be shorter in steeper basins
293 compared to shallower ones. This might influence the shape of pebbles as they tend to flatten as
294 effects of abrasion and 3D heterogeneities of bedrock that becomes more obvious with time and
295 transport distance (Sneed and Folk, 1958). We thus see the positive correlation between mean

296 basin hillslope angle and the sphericity of pebbles as a very likely consequence of shorter
297 transport times in steeper basins, but we note that this hypothesis needs to be confirmed by
298 detailed real-time surveys of material transport from sources down to the end of these rivers.

299

300 4.2 CONTROLS ON GRAIN SIZE

301 *Downstream fining trends in the Majes basin indicate fluvial controls*

302 In fluvial environments, the sorting of the sediment depends on the downstream distance from its
303 source (Hoey and Ferguson, 1994; Kodoma, 1994; Paola and Seal, 1995). This is particularly the
304 case for the Majes river, where we see an exponential downstream fining trend (Figure 4). This is
305 somewhat surprising because sufficiently voluminous sediment input from other sources may
306 perturb any downstream fining trends in the grain size distribution (Rice and Church, 1998).
307 Likewise, in the Majes basin, the sediment supply from the hillslopes to the trunk stream has
308 occurred mainly through debris flow processes and landsliding (Steffen et al., 2010; Margirier et
309 al., 2015). So, while the supply of hillslope-derived material is likely to have been accomplished
310 by mass wasting processes, its imprint on grain size appears to be modified by the evacuation
311 and the transport of this sediment down to the Pacific Ocean through fluvial transport.

312

313 *Grain size and earthquake impact*

314 Landslides and debris flows represent the main processes of hillslope erosion and the main
315 source of sediment in tectonically active orogens (Hovius et al., 1997; Korup et al., 2011). They
316 are generally associated with triggers such as earthquakes or intense rainfall and generally supply
317 coarse and voluminous sediments to the trunk rivers (Dadson et al., 2003; McPhillips et al.,
318 2014). In that sense, we would expect a positive correlation between the frequency of large

319 earthquakes and the grain size where an increase in earthquake frequency would induce an
320 increase in landslide occurrence, thereby supplying coarser grained sediment from the hillslopes
321 to the rivers. These relationships have been elaborated in multiples studies where positive
322 relationships between landslide occurrence and the size of earthquakes have been documented
323 (e.g., Keefer, 1984; 1994; Parker et al., 2011). We note that a global-scale correlation between
324 earthquake magnitudes and areas affected by landslides suggests that mass movements are
325 triggered by earthquakes if a threshold magnitude of 5.5 is exceeded (Keefer, 1984). Here, we
326 consider earthquakes with magnitudes >4.5 because Figure 1 by Keefer (1984) suggests that
327 earthquakes with magnitudes as low as 4.5 are theoretically able to release landslides over an
328 area larger than 10 km^2 . However, we do not see correlation between the number of recorded
329 historical earthquakes larger than 4.5 Mw and the grain size data (Figure 2c). We then expect
330 that the occurrence of earthquakes larger than 4.5 Mw, and related to this, the subduction
331 mechanisms, do not exert a measurable control on the grain size in the rivers of the western
332 Peruvian Andes.

333

334 *Possible threshold limits as controls on the grain size pattern*

335 The correlations between the grain size data and the basins scale properties (basin area, mean
336 basin denudation rates, water shear stresses, sediment fluxes) as rather weak and unconvincing
337 (Table 3). However, we recall that the D_{50} values record a nearly uniform pattern with values that
338 range between 2-3 cm along the studied western Peruvian margin. However, higher values of up
339 to 6 cm are either measured in streams where mean slope angles of the bordering hillslopes in the
340 upstream basin exceed 20° (between 11° and 12°S) or where water runoff values are nearly twice
341 as large as the mean of all Peruvian streams (ranging between $10\text{-}40 \text{ m}^3/\text{s}$ between 16° and 17°S ;

342 see Figure 3 and Table 3). Based on these observations, we tentatively interpret a supply control
343 on the median grain size for the Cordillera Negra streams where slopes are mediating grain size
344 through a threshold effect. In this case, these thresholds on the basin hillslope angles are likely to
345 be conditioned by the at-yield mechanical states of bedrock (Montgomery, 2001; Ouimet et al.,
346 2009), where hillslopes with dip angles up to 20-25° can be sustained. At these conditions,
347 hillslopes approach a threshold where slope angles are limited by the mechanical strength of
348 bedrock (Montgomery, 2001; Schlunegger et al., 2013). Hillslope erosion is then mainly
349 accomplished through mass failure processes, which dominate the supply of material to the trunk
350 and is likely to supply more coarse-grained material to the trunk stream, as modern examples
351 have shown (Bekaddour et al., 2013). In the same sense, a threshold response to steeper slopes
352 has been interpreted for the pattern of ¹⁰Be-based denudation rates in the Andes (Reber et al.,
353 2017) and in the Himalayas (Ouimet et al., 2009). In both cases, the relationships between
354 denudation rates and mean basin slopes was considered to follow a non-linear diffusive mass
355 transport model where denudation rates are proportional to mean basin slopes for low gradients,
356 while these relationships become non-linear for slopes approaching a critical value. Reber et al.
357 (2017) set this critical value to 27.5°, but the linear relationship of their dataset breaks apart for
358 gradients larger than 0.4, which corresponds to an angle of c. 21°. We note, however, that a
359 confirmation of this hypothesis requires data about the spatial density and frequency of landslide
360 occurrence along the western Peruvian Andes. This dataset, however, is not available yet, and its
361 establishment warrants further investigations.

362 In basins situated between 16°-17°S, mean basin slopes are clearly below threshold conditions,
363 but the D₅₀ values are twice as large as in neighboring rivers. Interestingly, these streams have
364 mean annual discharge values that are twice as large as the western Peruvian streams on the

365 average. Similar to the Cordillera Negra, we relate the relationships at 16°-17°S to threshold
366 controls. In this case, however, they are likely to be conditioned by transport. The mechanisms
367 by which grain size can be mediated through a threshold effect upon transport are less well
368 understood, but it has been known at least since the engineering work by Shields (1936), and
369 particularly by Peter Meyer Müller (1948) which has shown that threshold conditions have to be
370 exceeded and have a control on transport of grains in fluvial streams. As a consequence, at
371 transport-limited conditions, sediment flux, and most likely also the caliber of the transported
372 material, depends on the frequency and the magnitudes at which these thresholds are exceeded
373 rather than on a mean value of water discharge (Dadson et al., 2003). This might be the reason
374 why values of water shear stresses, that are calculated here based on the annual mean of water
375 flux, are not strongly correlated with the D_{50} values (Table 3). However, the lack of information
376 about discharge patterns prevents us from calculating the magnitude-frequency distribution of
377 runoff. Nevertheless, we consider the occurrence of large peak floods for streams that capture a
378 large portion of their waters on the Altiplano Plateau like this is the case for the Rio Ocoña and
379 Rio Camaña. We thus tentatively assign large peak floods for these streams, which might explain
380 the larger D_{50} values encountered in their gravel bars. Although highly speculative, we support
381 our statement by the highly seasonal character of precipitation occurrence particularly on the
382 eastern Andean margin and the Altiplano Plateau, which is largely conditioned by the monsoonal
383 Andean jet (see above). We note, however, that this statement warrants a high resolution
384 hydrological dataset for the western Peruvian streams, which is not available.

385 An exception from these relationships is presented by the Rio Santa (Figure 1A) where mean
386 annual water discharge reaches a value of almost $80 \text{ m}^3/\text{s}$, but where the size of the D_{50} is low.
387 We relate this to the possible supply-limited state of this stream, conditioned by the orogen-

388 parallel valley of the Rio Santa between the Cordillera Blanca and the Cordillera Negra, which
389 has acted as a subsiding graben since the past 5.4 Ma (Giovanni et al., 2010; Margirier et al.,
390 2015) and which might thus have operated as a sediment trap. This interpretation is also
391 consistent with the low ^{10}Be -based catchment averaged denudation rates measured for the Rio
392 Santa basin, as noted by Reber et al. (2017).

393 Note that our inferences are largely based on the pattern of the D_{50} , and that the consideration of
394 the larger percentiles might add alternative views on our interpretations. However, since all
395 percentiles are inter-correlated, as suggested by the pattern of the Pearson correlation coefficients
396 (Table 3), we think that our general conclusions about the occurrence of thresholds upon the
397 supply and transport of sediment will not change. Note also that either transport or supply control
398 and related thresholds were identified by Reber et al. (2017) for their explanation of the ^{10}Be -
399 based datasets on basin-averaged denudation rates on the western Peruvian Andes. We
400 tentatively interpret that the grain size pattern of the Peruvian streams follows these lines.

401

402 **Conclusion**

403 We present a complete dataset about grain sizes for all major rivers that are situated on the
404 western Andean margin of Peru. We did not find any correlations to the current seismic regimes,
405 where a larger occurrence of earthquakes with magnitudes larger than 4.5 Mw is expected to
406 increase the supply of coarse-grained material. However, we found that the values for the D_{50} are
407 nearly constant and range between 2 and 3 cm. Exceptionally larger D_{50} values of 4-6 cm were
408 measured for basins situated between 11-12°S and 16-17°S where hillslope gradients are steeper
409 than average (i.e., 20-22°), or where mean annual stream flows exceed the average values of the
410 western Peruvian streams (10-40 m^3/s) by a factor of 2. We suggest that the generally uniform

411 grain size pattern has been perturbed where either mean basin slopes, or water fluxes exceed
412 threshold conditions upon the supply and the transport of material. This might have implications
413 for our understanding of the controls on the grain size distribution of gravelly-based streams.

414

415 **ACKNOWLEDGMENTS**

416 This project is funded by the Swiss National Science Foundation (project Number 137516). We
417 thank the associate editor Robert Hilton and editor Andreas Lang for handling the manuscript
418 and the referees for their constructive comments.

419

420 **REFERENCES CITED**

421 Abbühl, L.M., Norton, K.P., Jansen, J.D., Schlunegger, F., Aldahan, A., and Possnert, G., 2011,
422 Erosion rates and mechanisms of knickzone retreat inferred from ¹⁰Be measured across
423 strong climate gradients on the northern and central Andes Western Escarpment: *Earth
424 Surface Processes and Landforms*, v. 36, p. 1464–1473.

425 Allen, G. H., Barnes, J. B., Pavelsky, T. M. and Kirby, E., 2013, Lithologic and tectonic controls
426 on bedrock channel form at the northwest Himalayan front: *Journal of Geophysical
427 Research: Earth Surface*, v. 118, no. 3, p. 1806-1825.

428 Allen, P.A., Armitage, J.J., Whittaker, A.C., Michael, N.A., Roda-Boluda, D. and D’Arcy, M.,
429 2015, Fragmentation model of the grain size mix of sediment supplied to basins: *The
430 Journal of Geology*, v. 123, p. 405-427.

431 Allen, P. A., Michael, N. A., D’Arcy, M., Roda-Boluda, D. C., Whittaker, A. C., Duller, R. A.,
432 and Armitage, J. J., 2016. Fractionation of grain size in terrestrial sediment routing
433 systems. *Basin Research*. v. 29(2), p. 180-202

434 Atherton, M. P., 1984. The coastal batholith of Peru. In *Andean Magmatism* (pp. 168-179).
435 Birkhäuser Boston.

436 Attal, M. and Lavé, J., 2006, Changes of bedload characteristics along the Marsyandi River
437 (central Nepal): Implications for understanding hillslope sediment supply, sediment load

- 438 evolution along fluvial networks, and denudation in active orogenic belts: Geological
439 Society of America Special Papers, v. 398, p.143-171.
- 440 Attal, M. and Lavé, J., 2009. Pebble abrasion during fluvial transport: experimental results and
441 implications for the evolution of the sediment load along rivers. *J. Geophys. Res.*
442 114:F04023. doi:10.1029/2009JF001328.
- 443 Attal, M., Mudd, S. M., Hurst, M. D., Weinman, B., Yoo, K. and Naylor, M., 2015, Impact of
444 change in erosion rate and landscape steepness on hillslope and fluvial sediments grain
445 size in the Feather River basin (Sierra Nevada, California): *Earth Surface Dynamics*, v. 3,
446 p. 201-222.
- 447 Bekaddour, T., Schlunegger, F., Attal, M. and Norton, K. P., 2013. Lateral sediment sources and
448 knickzones as controls on spatio-temporal variations of sediment transport in an Alpine
449 river. *Sedimentology*, v. 60(1), p. 342-357.
- 450 Blissenbach, E., 1952. Relation of surface angle distribution to particle size distribution on
451 alluvial fans: *J. Sediment. Petrol.*, v. 22, p. 25–28.
- 452 Bookhagen, B. and Strecker, M. R., 2008, Orographic barriers, high-resolution TRMM rainfall,
453 and relief variations along the eastern Andes, *Geophysical Research Letters*, v. 35, p.
454 L06403.
- 455 Bourgois, J., Bigot-Cormier, F., Bourles, D., Braucher, R., Dauteuil, O., Witt, C., & Michaud, F.,
456 2007. Tectonic record of strain buildup and abrupt coseismic stress release across the
457 northwestern Peru coastal plain, shelf, and continental slope during the past 200 kyr.
458 *Journal of Geophysical Research: Solid Earth*, 112(B4).
- 459 Bunte, K., Abt, S.R., 2001a. Sampling frame for improving pebble count accuracy in coarse
460 gravel-bed rivers. *Journal of the American Water Resources Association*, v. 37 (4), p.
461 1001- 1014.
- 462 Bunte, K., Abt, S.R., 2001b. Sampling surface and subsurface particle-size distributions in
463 wadable gravel- and cobble-bed rivers for analyses in sediment transport, hydraulics,
464 and streambed monitoring. General Technical Report RMRS-GTR-74. United States
465 Department of Agriculture; Forest Service; Rocky Mountain Research Station. Fort
466 Collins, USA, p. 428.
- 467 Carretier, S., Tolorza, V., Rodríguez, M. P., Pepin, E., Aguilar, G., Regard, V. and Hérail, G.,
468 2015. Erosion in the Chilean Andes between 27° S and 39° S: tectonic, climatic and

- 469 geomorphic control. Geological Society, London, Special Publications, v. 399(1), p. 401-
470 418.
- 471 Dadson, S. J., Hovius, N., Chen, H., Dade, W. B., Hsieh, M. L., Willett, S. D. and Lague, D.,
472 2003. Links between erosion, runoff variability and seismicity in the Taiwan orogen.
473 Nature, v. 426(6967), p. 648-651.
- 474 D'arcy, M., Whittaker, A. C., and Roda-Boluda, D. C., 2017. Measuring alluvial fan sensitivity
475 to past climate changes using a self-similarity approach to grain-size fining, Death
476 Valley, California. Sedimentology, v. 64(2), p. 388-424.
- 477 DeVries, T. J., 1987, A review of geological evidence for ancient El Nino activity in Peru. J.
478 Geophys. Res, v. 92, no. 14, p. 471–14.
- 479 Dingle, E. H., Attal, M., and Sinclair, H. D., 2017. Abrasion-set limits on Himalayan gravel flux.
480 Nature, v. 544(7651), p. 471-474.
- 481 Duller, R. A., Whittaker, A. C., Swinehart, J. B., Armitage, J. J., Sinclair, H. D., Bair, A. and
482 Allen, P. A., 2012, Abrupt landscape change post-6 Ma on the central Great Plains,
483 USA: Geology, v. 40, p. 871-874.
- 484 Fedele, J. J. and Paola C., 2007, Similarity solutions for fluvial sediment fining by selective
485 deposition: Journal of Geophysical Research: Earth Surface (2003–2012), v. 112.
- 486 Foreman, B. Z., Heller, P. L. and Clementz, M. T., 2012, Fluvial response to abrupt global
487 warming at the Palaeocene/Eocene boundary: Nature, v. 491, no. 7422, p. 92-95
- 488 Foreman, B. Z., 2014, Climate-driven generation of a fluvial sheet sand body at the Paleocene–
489 Eocene boundary in north-west Wyoming (USA): Basin Research, v. 26, no. 2, p. 225-
490 241.
- 491 Garreaud, R. D., Vuille, M., Compagnucci, R., and Marengo, J., 2009, Present-day South
492 American climate. Palaeogeography, Palaeoclimatology, Palaeoecology, v. 281, no. 3, p.
493 180-195.
- 494 Haederle, M. and Atherton, M. P., 2002. Shape and intrusion style of the Coastal Batholith, Peru.
495 Tectonophysics, v. 345(1), p. 17-28.
- 496 Hancock, G. S. and Anderson, R. S., 2002. Numerical modeling of fluvial strath-terrace
497 formation in response to oscillating climate. Geological Society of America Bulletin, v.
498 114(9), p. 1131-1142.

- 499 Heller, P. L. and Paola, C., 1992, The large-scale dynamics of grain-size variation in alluvial
500 basins, 2: Application to syntectonic conglomerate: *Basin Research*, v. 4, no. 2, p. 91-
501 102.
- 502 Hjulström, F., 1935, Studies in the morphological activity of rivers as illustrated by the river
503 Fyris: *Bulletin of the Geological Institution of the University of Uppsala*, v 25, p. 221-
504 528.
- 505 Hoey, T. B. and Ferguson, R., 1994, Numerical simulation of downstream fining by selective
506 transport in gravel bed rivers: Model development and illustration: *Water resources*
507 *research*, v.30, p. 2251-2260.
- 508 Hovius, N., Stark, C. P. and Allen, P. A., 1997. Sediment flux from a mountain belt derived by
509 landslide mapping. *Geology*, v. 25(3), p. 231-234.
- 510 Howard, J.L., 1993. The statistics of counting clasts in rudites: a review with examples from the
511 upper Paleogene of southern California, USA. *Sedimentology* 40, 157-174.
- 512 Huffman, G. J., Bolvin, D. T., Nelkin, E. J., Wolff, D. B., Adler, R. F., Gu, G. and Stocker, E. F.,
513 2007, The TRMM multisatellite precipitation analysis (TMPA): Quasi-global, multiyear,
514 combined-sensor precipitation estimates at fine scales. *Journal of Hydrometeorology*, v.
515 8, no. 1, p. 38-55.
- 516 Isacks, B. L., 1988. Uplift of the central Andean plateau and bending of the Bolivian orocline.
517 *Journal of Geophysical Research: Solid Earth*, v. 93(B4), p. 3211-3231.
- 518 Keefer, D. K., 1984. Landslides caused by earthquakes. *Geological Society of America Bulletin*,
519 v. 95(4), p. 406-421.
- 520 Kodoma, Y., 1994, Downstream changes in the lithology and grain size of fluvial gravels, the
521 Watarase River, Japan: Evidence of the role of abrasion in downstream fining: *Journal of*
522 *Sedimentary Research, Section A: Sedimentary Petrology and Processes*, v. 64A, p. 68-
523 75.
- 524 Koiter, A. J., Owens, P. N., Peticrew, E. L. and Lobb, D. A., 2013, The behaviour characteristics
525 of sediment properties and their implications for sediment fingerprinting as an approach
526 for identifying sediment source sin river basins: *Earth Science Reviews*, v. 125, p. 24-42.
- 527 Korup, O. and Schlunegger, F., 2009. Rock-type control on erosion-induced uplift, eastern Swiss
528 Alps. *Earth and Planetary Science Letters*, v. 278(3), p. 278-285.

- 529 Korup, O. and Weidinger, J. T., 2011. Rock type, precipitation, and the steepness of
530 Himalayan threshold hillslopes. Geological Society, London, Special Publications, v.
531 353(1), p. 235-249.
- 532 Lisle, T.E., Iseya, F. and Ikeda, H., 1993, Response of a channel with alternate bars to a
533 decrease in supply of mixed-size bed load: A flume experiment: Water resources
534 research, v. 29, p. 3623–3629.
- 535 Litty, C., Duller, R., and Schlunegger, F., 2016. Paleohydraulic reconstruction of a 40 ka-old
536 terrace sequence implies that water discharge was larger than today. Earth surface
537 processes and landforms.
- 538 Litty, C., Lanari, P., Burn, M., and Schlunegger, F., 2017, Climate-controlled shifts in sediment
539 provenance inferred from detrital zircon ages, Western Peruvian Andes. *Geology*. v. 45;
540 no. 1; p. 59–62.
- 541 Macharé, J., & Ortlieb, L., 1992. Plio-Quaternary vertical motions and the subduction of the
542 Nazca Ridge, central coast of Peru. *Tectonophysics*, v. 205(1-3), p. 97-108.
- 543 Marcus, W.A., Ladd, S.C., Stoughton, J.A., Stock, J.W., 1995. Pebble counts and the role of
544 user-dependent bias in documenting sediment size distributions. *Water Resources*
545 *Research*, v. 31 (10), p. 2625-2631.
- 546 Margirier, A., Robert, X., Audin, L., Gautheron, C., Bernet, M., Hall, S., Simon-Labric, T., 2015.
547 Slab flattening, magmatism, and surface uplift in the Cordillera Occidental (northern Peru).
548 *Geology*, v. 43, p. 1031-1034.
- 549 McLaren, P. and Bowles, D., 1985, The Effects of Sediment Transport on Grain-Size
550 Distributions: *Journal of Sedimentary Petrology*, v. 55, p. 457-470.
- 551 McNulty, B., & Farber, D., 2002. Active detachment faulting above the Peruvian flat slab.
552 *Geology*, v. 30(6), p. 567-570.
- 553 McPhillips, D., Bierman, P. R., & Rood, D. H., 2014. Millennial-scale record of landslides in the
554 Andes consistent with earthquake trigger. *Nature Geoscience*, v. 7(12), p. 925-930.
- 555 Meyer-Peter, E., & Müller, R., 1948. Formulas for bed-load transport. In IAHSR 2nd meeting,
556 Stockholm, appendix 2. IAHR.
- 557 Montgomery, D., 2001. Slope distributions, threshold hillslopes, and steady-state topography.
558 *American Journal of Science*, v. 301, p. 432-454.

- 559 Montgomery, D. R., Balco, G. and Willett, S. D., 2001. Climate, tectonics, and the morphology
560 of the Andes. *Geology*, v. 29(7), p. 579-582.
- 561 Mukasa, S. B., 1986. Zircon U-Pb ages of super-units in the Coastal batholith, Peru: Implications
562 for magmatic and tectonic processes. *Geological Society of America Bulletin*, v. 97(2), p.
563 241-254.
- 564 Nocquet, J. M., Villegas-Lanza, J. C., Chlieh, M., Mothes, P. A., Rolandone, F., Jarrin, P. and
565 Martin, X., 2014. Motion of continental slivers and creeping subduction in the northern
566 Andes. *Nature Geoscience*, v. 7(4), p. 287-291.
- 567 Noury, M., Bernet, M., Schildgen, T. F., Simon-Labric, T., Philippon, M., & Sempere, T., 2016.
568 Crustal-scale block tilting during Andean trench-parallel extension: Structural and geo-
569 thermochronological insights. *Tectonics*, v. 35(9), p. 2052-2069.
- 570 Ouimet, W. B., Whipple, K. X., & Granger, D. E., 2009. Beyond threshold hillslopes: Channel
571 adjustment to base-level fall in tectonically active mountain ranges. *Geology*, v. 37(7), p.
572 579-582.
- 573 Paola, C., Heller, P. L. and Angevinet, C. L., 1992a, The large-scale dynamics of grain-size
574 variation in alluvial basins, 1: Theory: *Basin Research*, v. 4, p. 73-90.
- 575 Paola, C. and Seal, R., 1995, Grain size patchiness as a cause of selective deposition and
576 downstream fining: *Water Resources Research*, v. 31, p. 1395-1407.
- 577 Parker, G., 1991, Selective sorting and abrasion of river gravel. 1: Theory: *Journal of*
578 *Hydraulic Engineering*, v. 117, no. 2, p. 131-147.
- 579 Parker, R. N., Densmore, A. L., Rosser, N. J., De Michele, M., Li, Y., Huang, R. & Petley, D.
580 N., 2011. Mass wasting triggered by the 2008 Wenchuan earthquake is greater than
581 orogenic growth. *nature geoscience*, v. 4(7), p. 449-452.
- 582 Pearson, K., 1895, Notes on regression and inheritance in the case of two parents, *Proceedings of*
583 *the Royal Society of London*, v. 58, p. 240–242.
- 584 Ramos, V. A., 2010. The tectonic regime along the Andes: Present-day and Mesozoic regimes.
585 *Geological Journal*, v. 45(1), p. 2-25.
- 586 Rasband, W.S., ImageJ, U. S. National Institutes of Health, Bethesda, Maryland, USA,
587 <http://imagej.nih.gov/ij/>, 1997-2016.

- 588 Reber, R., Delunel, R., Schlunegger, F., Litty, C., Madella, A., Akçar, N., Christl, M.
589 Environmental controls on ¹⁰Be-based catchment averaged denudation rates along the
590 western margin of the Peruvian Andes. *Terra Nova*.
- 591 Regard, V., Saillard, M., Martinod, J., Audin, L., Carretier, S., Pedoja, K. and Hérail, G., 2010.
592 Renewed uplift of the Central Andes Forearc revealed by coastal evolution during the
593 Quaternary. *Earth and Planetary Science Letters*, v. 297(1), p. 199-210.
- 594 Reuter, H. I., Nelson, A. and Jarvis, A., 2007. An evaluation of void-filling interpolation
595 methods for SRTM data. *International Journal of Geographical Information Science*, v.
596 21(9), p. 983-1008.
- 597 Rice, S. and Church, M., 1998, Grain size along two gravel-bed rivers: Statistical variation,
598 spatial pattern and sedimentary links: *Earth Surface Processes and Landforms*, v. 23, p.
599 345-363.
- 600 Robinson, R. A. and Slingerland, R. L., 1998, Origin of fluvial grain-size trends in a foreland
601 basin: the Pocono Formation on the central Appalachian basin: *Journal of Sedimentary*
602 *Research*, v. 68, no. 3.
- 603 Schildgen, T. F., Hodges, K. V., Whipple, K. X., Reiners, P. W. and Pringle, M. S., 2007, Uplift
604 of the western margin of the Andean plateau revealed from canyon incision history,
605 southern Peru. *Geology* 35, 523–526.
- 606 Schlunegger, F., Norton, K.P., Caduff, R., 2013. Hillslope processes in temperate environments.
607 In: John F. Shorder (ed.): *Treatise on Geomorphology*, v. 7: p. 337-345, San Diego:
608 Academic Press.
- 609 Schumm, S. A. and Stevens, M. A., 1973, Abrasion in place: a mechanism for rounding and size
610 reduction of coarse sediments in rivers: *Geology*, v. 1, p. 37-40.
- 611 Sébrier, M., Mercier, J. L., Macharé, J., Bonnot, D., Cabrera, J., & Blanc, J. L., 1988. The state
612 of stress in an overriding plate situated above a flat slab: The Andes of central Peru.
613 *Tectonics*, v. 7(4), p. 895-928.
- 614 Shields, A., 1936, Anwendung der Ähnlichkeitsmechanik und der Turbulenzforschung auf die
615 Geschiebebewegung, Mitteilung der preussischen Versuchsanstalt für Wasserbau und
616 Schiffbau, 26. (Berlin).
- 617 Sneed, E.D., and Folk, R.L., 1958. Pebbles in the lower Colorado River, Texas a study in particle
618 morphogenesis. *The Journal of Geology*, 114-150.

- 619 SNIRH; Sistema Nacional de Informacion de Recursos Hidricos. [http://snirh.ana.gob.](http://snirh.ana.gob.pe/consultasSnirh/ConsHidrom2.aspx)
620 [pe/consultasSnirh/ConsHidrom2.aspx](http://snirh.ana.gob.pe/consultasSnirh/ConsHidrom2.aspx)
- 621 Steffen, D., Schlunegger, F., and Preusser, F., 2010, Late Pleistocene fans and terraces in the
622 Majes valley, southern Peru, and their relation to climatic variations. *International*
623 *Journal of Earth Sciences*, v. 99(8), p. 1975-1989.
- 624 Sternberg, H., 1875, Untersuchungen über längen-und Querprofil geschiebeführender Flüsse, *Z.*
625 *Bauwes.*, 25, 486–506.
- 626 Surian, N., 2002, Downstream variation in grain size along an Alpine river: analysis of
627 controls and processes: *Geomorphology*, v. 43, p. 137-149.
- 628 Trauerstein, M., Norton, K. P., Preusser, F., and Schlunegger, F., 2013, Climatic imprint on
629 landscape morphology in the western escarpment of the Andes. *Geomorphology*, v. 194,
630 p. 76-83.
- 631 Vidal, J. C., 1993, *Geologia de los cuadrangulos de Huambo y Orcopampa*, v 46. Instituto
632 Geologico Minero y Metalurgico, Lima.
- 633 Whittaker, A. C., Cowie, P. A., Attal, M., Tucker, G. E. and Roberts, G. P., 2007, Bedrock
634 channel adjustment to tectonic forcing: Implications for predicting river incision rates:
635 *Geology*, v. 35, no. 2, p.103-106.
- 636 Whittaker, A. C., Attal, M. and Allen, P.A., 2010, Characterising the origin, nature and fate of
637 sediment exported from catchment perturbed by active tectonics. *Basin Research*. v. 22. p.
638 809-828.
- 639 Wittmann, H., von Blanckenburg, F., Kruesmann, T., Norton, K. P., and Kubik, P. W., 2007.
640 Relation between rock uplift and denudation from cosmogenic nuclides in river sediment
641 in the Central Alps of Switzerland. *Journal of Geophysical Research: Earth Surface*,
642 112(F4).

643

644

645 **FIGURES AND TABLES CAPTIONS**

646

647 **Table 1:** Location of the sampling sites with the altitude in meters above sea level. The table also
648 displays grain size results together with the rivers' and basins' properties and hydrological
649 properties.

650

651 **Table 2:** Location of the sampling sites in the Majes basin and grain size results in the Majes
652 basin.

653

654 **Table 3:** Results of the statistical investigations, illustrated here as correlation matrix of the r-
655 values. The values in bold show significant correlation between the grain size data and the
656 different catchment scale properties.

657

658

659 **Figure 1: A:** Map of the studied basins showing the sampling sites and the western escarpment
660 (western escarpment modified after Trauerstein et al., 2013). The purple strip east of the trench
661 axis corresponds to the swath over which the historical earthquake data, presented in Figure 3,
662 The map also illustrates the location of the buoyant Nazca ridge, depth of the slab in dashed line,
663 plus patterns of earthquake occurrence. **B:** Geological map of the western Peruvian Andes. **C:**
664 Map of the precipitation rates showing the spatial extent of the ITCZ, modified after Huffman et
665 al., 2007.

666

667

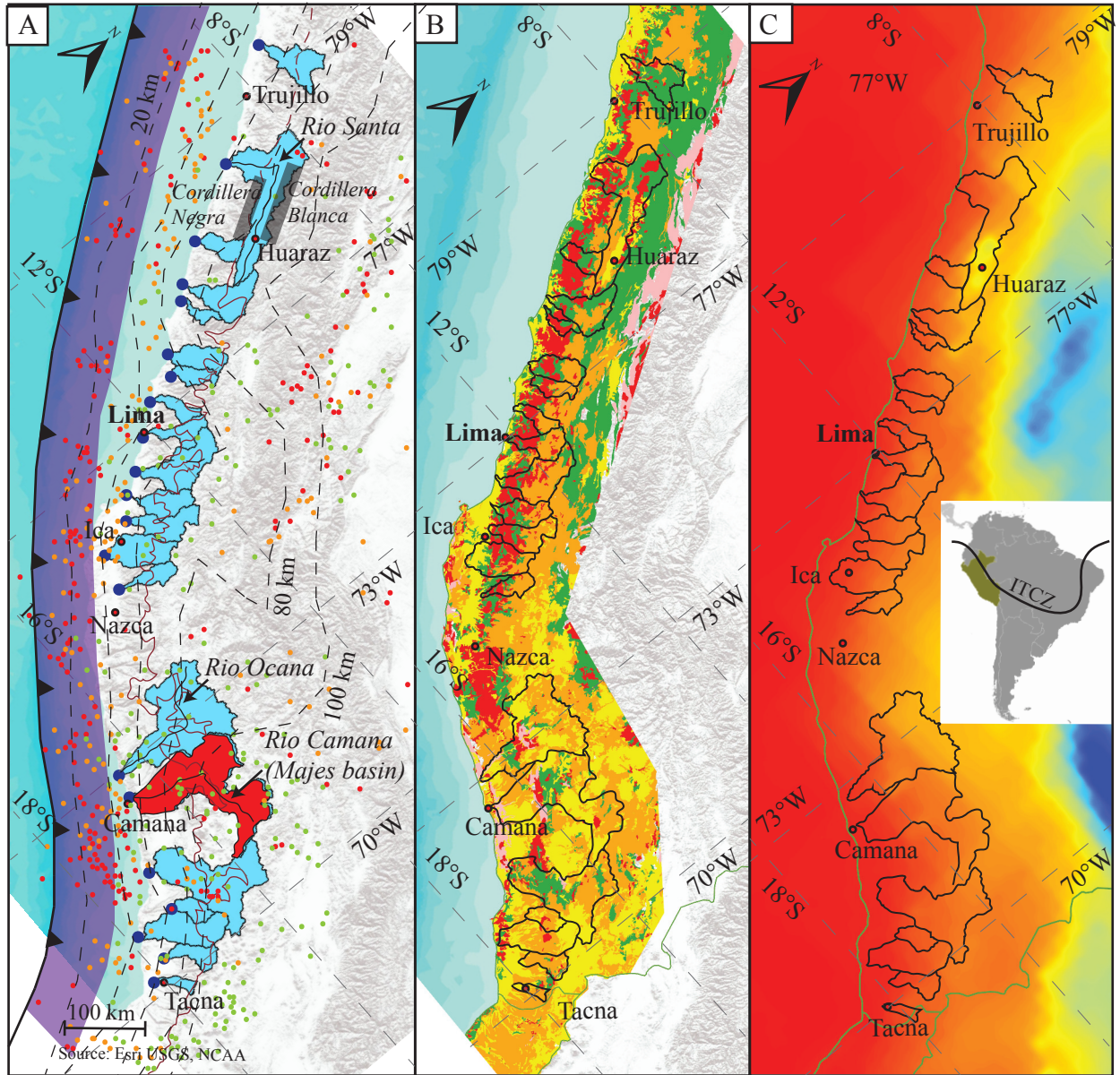
668 **Figure 2:** Topography of subducting Nazca plate, where slab depth data has been extracted from
669 earthquake.usgs.gov/data/slab/ modified from Reber et al., 2017. This N-S projection also

670 illustrates: a) tectonic lineaments such as submarine ridges and MFZ: Mendaña Fracture Zone;
671 NFZ: Nazca Fracture Zone; b) Holocene Volcanoes; c) Earthquake data, taken from
672 earthquake.usgs.gov/earthquakes/search/; number of earthquakes $M > 4$ within 30 km radius
673 window. d) Coastal elevation. The data has been extracted from a 20 km-wide swath profile along
674 the coast. The three lines represent maximum, mean and minimum elevations within the selected
675 swath; e) Catchment averaged denudation rates have been corrected for quartz contents (Reber et
676 al. 2017); f) Mean annual precipitation rates (Reber et al., 2017); g) Mean annual water discharge
677 (Reber et al., 2017); h) Grain size results for the intermediate (b)-axis of the pebbles in the rivers
678 from north to south at the sampling sites presented in Figure 1; i) Ratio between the intermediate
679 axis and the long (a)-axis (modified after Reber et al., 2017). Exceptionally larger D_{50} values of 4-
680 6 cm were measured for basins situated between 11-12°S and 16-17°S where hillslope gradients
681 are steeper than 0.4 on the average (i.e., 20-22°), or where mean annual stream flows exceed the
682 average values of the western Peruvian streams (10-40 m³/s) by a factor of 2.

683
684 **Figure 3:** Geological map of the Majes basin overlain by the precipitation pattern (Precipitation
685 data from Steffen et al., 2010), where the black dashed lines show precipitation rates (mm/yr).
686 GS1 to GS5 represent sites where grain size data has been collected. The right corner shows the
687 Majes river long profile.

688
689 **Figure 4:** Grain size results along the Majes River.

690

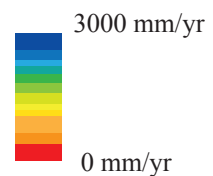


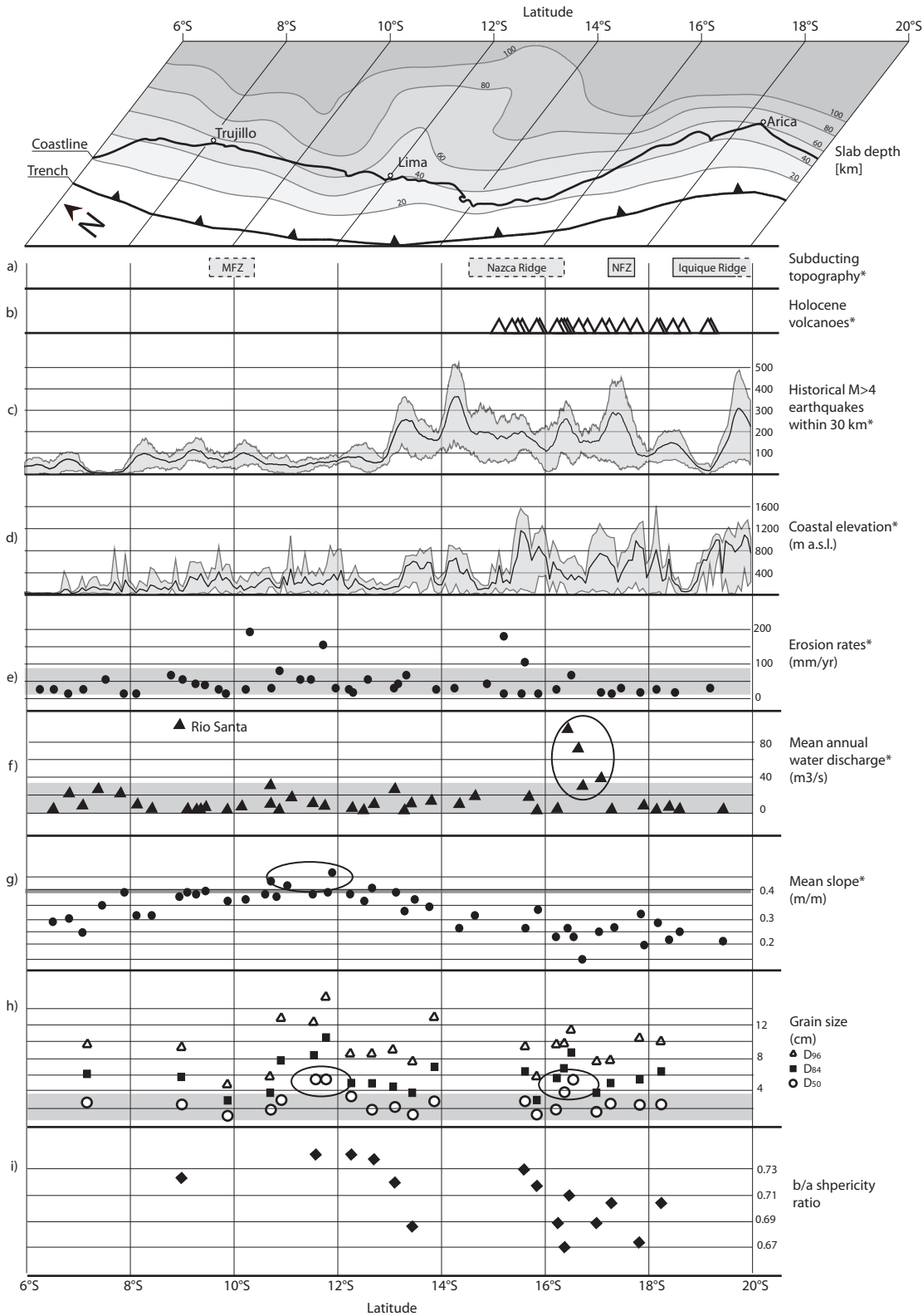
- Multiple sampled basin
- Studied basins
- Sampling site
- City
- Western escarpment
- USGS earthquake archive (Mag > 4.5)
- Depth (km)
 - 0 - 33
 - 33 - 70
 - 70 - 300
- trench axis

Geology

- Quaternary deposits
- Cenozoic rocks
- Coastal batholith
- Mesozoic rocks
- Metamorphic rocks

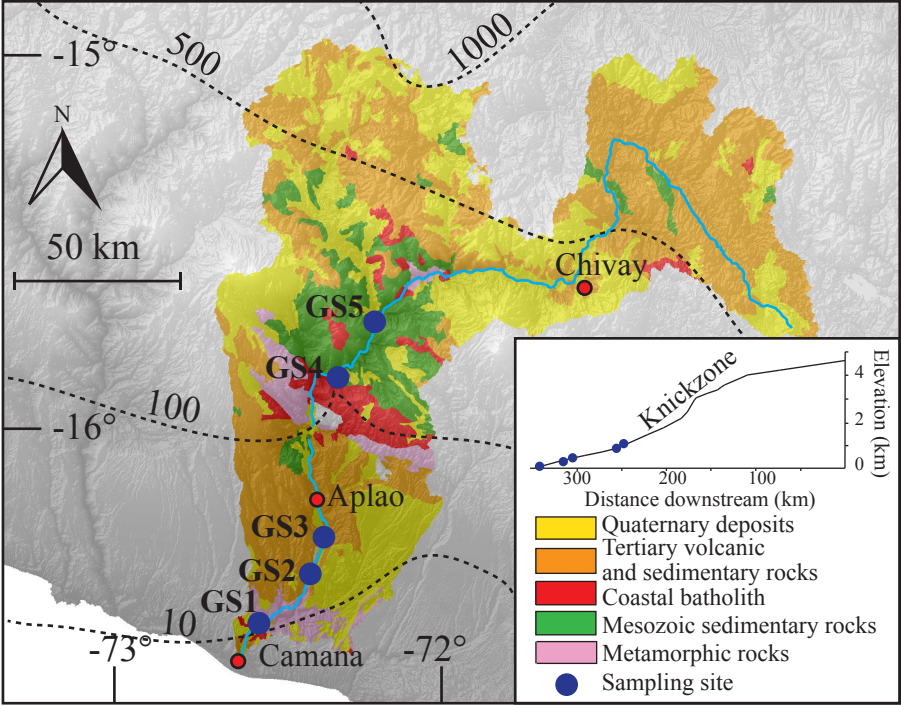
Annual precipitations TRMM





Base level in the data
 Threshold of mean catchment slope of 20°

Higher value than base level
 * Data from Reber et al. (2017)



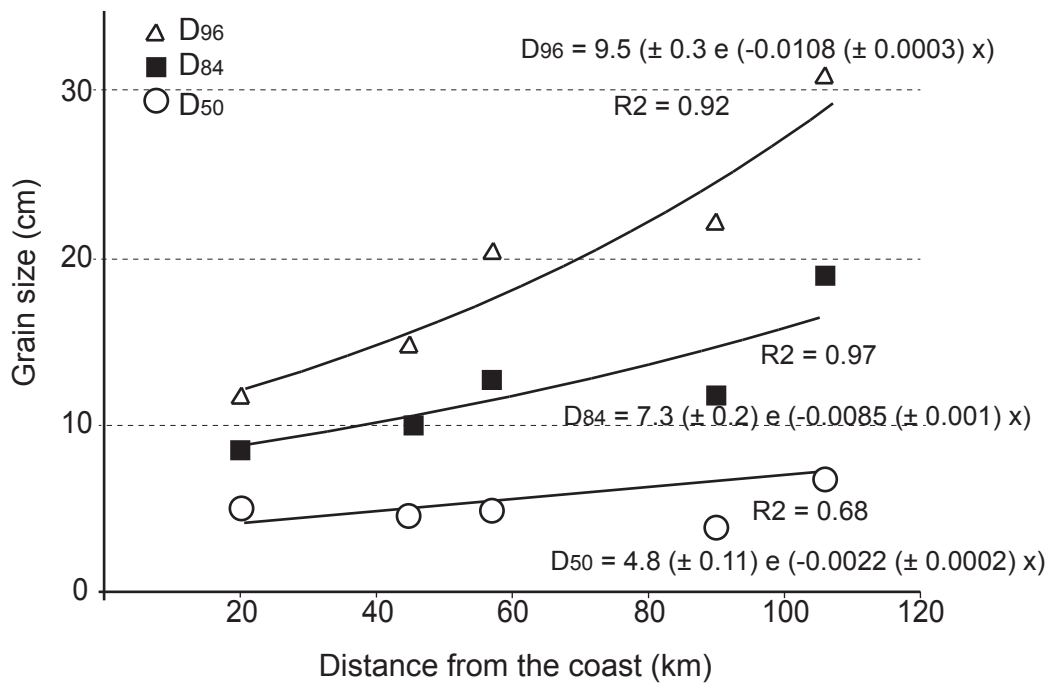


Figure 4: Grain size results along the Majes River.

River name	Sample name	Altitude (m)	Latitude (DD WGS84)	Longitude (DD WGS84)	D50 (cm)	D84 (cm)	D96 (cm)	b/a	Catchment area (km ²)	Mean basin slope (m/m) (Reber et al., 2017)	Slope at the sampling site (m/m)	Distance from the western escarpment (km)	Channel width at the sampling site (m)	Mean annual water discharge (m ³ /s) (Reber et al., 2017)	Shear stress (kg/m.s ²)	Sediment flux (m ³ /s)	Denudation rates (mm/ka) (Reber et al., 2017)	Denudation rates uncertainties (mm/ka) (Reber et al., 2017)	Denudation rates corrected for Qz content in bedrock (mm/ka) (Reber et al., 2017)
Tacna	PRC-ME1	231	-18.12	-70.33	2.3	6.2	10.0	0.70	899	0.28	0.015	48	6	3.4	142.68	11952	13.3	3.6	12.2
Rio Sama Grande	PRC-ME3	455	-17.82	-70.51	2.5	5.5	10.6	0.67	2150	0.3	0.013	73	6	4	114.14	61495	28.6	5.3	27.7
Ilo / Rio Osmore	PRC-ME5	1072	-17.29	-70.99	2.6	5.1	7.8	0.70	1783	0.26	0.018	53	7	3.4	184.18	38146	21.4	4.8	18.6
Rio Tambo	PRC-ME6	145	-17.03	-71.69	1.5	3.6	7.5	0.69	12885	0.24	0.051	141	26	38.1	265.69	1155744	89.7	16.7	72.1
Tambillo / Rio Sihuas	PRC-ME802	117	-16.34	-72.13	2.0	6.0	10.0	0.69	1708	0.15	0.019	70	15	30.1	88.78	58087	34	6.4	27.7
Camana / Rio Majes	PRC-ME7	69	-16.51	-72.64	5.2	8.7	11.6	0.67	17401	0.23	0.005	188	100	68.4	46.06	2218568	127.5	23.4	106.8
Ocona / Rio Ocona	PRC-ME9	14	-16.42	-73.12	4.8	6.8	10.0	0.71	16084	0.26	0.004	192	70	91.1	26.25	3893878	242.1	45	184.1
Nasca / Rio Grande	PRC-ME1402	15	-15.85	-74.26	1.3	3.0	6.0	0.71	1412	0.32	0.014	48	3	20.4	34.10	65093	46.1	8.6	29.4
Chacaltana / Rio Ica	PRC-ME15	3	-15.63	-74.64	2.9	6.4	9.6	0.73	4677	0.26	0.003	88	23	12.1	33.01	126266	27	5.7	25.1
Humay District / Rio Pischo	PRC-ME16	400	-13.73	-75.89	3	6.6	13		3649	0.34	0.013	62	20	13.6	112.91	379865	104.1	20.4	69.1
Chinca Alta / Rio San Juan	PRC-ME17	75	-13.47	-76.14	1.3	3.8	7.6	0.69	3090	0.37	0.01	78	5	10.1	48.54	189112	61.2	11.7	44.1
Rio Canete	PRC-ME19	23	-13.12	-76.39	2	4.6	8.8	0.72	6029	0.4	0.01	100	60	26.4	112.24	402743	66.8	12.3	51.2
Rio Omas	PRC-ME20	33	-12.67	-76.65	1.6	4.8	8.8	0.73	2322	0.41	0.0076	78	22	8.2	95.14	62913	27.1	5.4	17.9
Rio Lurin	PRC-ME22	40	-12.25	-76.89	3	5	8.8	0.74	1572	0.38	0.022	70	5	3.7	176.26	60515	38.5	7.1	23.6
Lima / Rio Chillon	PRC-ME39	402	-11.79	-76.99	5.3	10.5	15.5		1755	0.39	0.018	51	40	4.9	392.89	144272	82.2	15.5	53.4
Rio Chancay	PRC-ME23	72	-11.61	-77.24	5.5	8.3	12.5	0.74	3059	0.39	0.01	66	20	8.9	111.55	298866	97.7	18.4	52.8
Rio Supe	PRC-ME25	74	-11.07	-77.59	2.8	7.7	13		4306	0.38	0.012	82	5	3.8	98.55	179550	41.7	7.7	25.6
Rio Pativilca	PAT-ME	10	-10.72	-77.77	1.8	3.6	6		4607	0.44	0.014	74	30	30.9	96.30	1198281	260.1	48.8	190.9
Huarmey	PRC-ME38	24	-10.07	-78.16	1.7	3.4	5.2		2072	0.37	0.004	78	15	9.8	38.34	40816	19.7	4.5	10.1
Rio Santa	PRC-ME27	80	-8.97	-78.62	2	5.4	9	0.72	12313	0.38	0.005	65	40	96.1	23.08	876699	71.2	13.4	70.4
San Martin de Porres	PRC-ME30	67	-7.32	-79.48	2.9	6.3	10		3882	0.34	0.007	126	40	25.4	65.72	118401	30.5	5.9	25.8

Table 1 : Location of the sampling sites with the altitude in meters above sea level.
The table also displays grain size results together with the rivers' and basins' properties and hydrological properties.
Morphometric dataset for the sampled drainage basins. All calculations are based on the 90 m resolution DEM (NASA)
The precipitation, water discharge data and the denudation rates are from Reber et al., in review

	Distance from the coast (km)	Altitude (m)	Latitude (°)	Longitude (°)	D50	D84	D96	b/a
GS1	20	69	-16.51	-72.64	5.2	8.7	11.6	0.67
GS2	45	283	-16.37	-72.49	4.8	10	15	0.69
GS3	57	378	-16.28	-72.45	5.4	12.7	21	0.65
GS4	90	700	-16.00	-72.48	3.3	12	22.5	0.67
GS5	106	882	-15.86	-72.45	6.2	19	31	0.71

Table 2: Location of the sampling sites in the Majes basin and grain size results in the Majes basin.

	Altitude (m)	Latitude (DD WGS84)	Longitude (DD WGS84)	D50 (cm)	D84 (cm)	D96 (cm)	b/a	Catchment area (km ²)	Mean slope (m/m)	Distance form the western escarpment (km)	Mean annual water discharge (m ³ /s)	Shear stress (kg/m.s ²)	Sediment flux (m ³ /s)	Denudation rates (mm/ka)	Denudation rates corrected for Qz content in bedrock (mm/ka)	
Altitude (m)	1.00															
Latitude (DD WGS84)	-0.36	1.00														
Longitude (DD WGS84)	0.46	-0.97	1.00													
D50 (cm)	0.09	0.00	-0.01	1.00												
D84 (cm)	0.14	0.04	-0.03	0.87	1.00											
D96 (cm)	0.18	0.02	-0.02	0.73	0.93	1.00										
b/a	-0.30	0.66	-0.71	0.09	0.00	-0.02	1.00									
Catchment area (km ²)	-0.25	-0.12	0.12	0.31	0.16	0.04	-0.25	1.00								
Mean slope (m/m)	-0.23	0.72	-0.78	-0.07	-0.10	-0.03	0.63	-0.28	1.00							
Distance form the western escarpment (km)	-0.32	-0.14	0.14	0.35	0.16	0.03	-0.33	0.84	-0.35	1.00						
Mean annual water discharge (m ³ /s) (Reber et al., 2017)	-0.30	0.03	-0.01	0.18	0.05	-0.07	-0.13	0.87	-0.23	0.64	1.00					
Shear stress (kg/m.s ²)	0.45	-0.11	0.14	0.23	0.33	0.39	-0.06	-0.21	0.06	-0.23	-0.37	1.00				
Sediment flux (m ³ /s)	-0.23	-0.19	0.17	0.42	0.17	0.03	-0.21	0.86	-0.24	0.82	0.80	-0.22	1.00			
Denudation rates (mm/ka) (Reber et al., 2017)	-0.23	0.04	-0.09	0.34	0.09	0.00	-0.09	0.56	0.12	0.48	0.56	-0.07	0.79	1.00		
Denudation rates corrected for Qz content in bedrock (mm/ka) (Reber et al., 2017)	-0.22	0.01	-0.04	0.30	0.06	-0.03	-0.17	0.64	0.05	0.54	0.65	-0.11	0.84	0.99	1.00	

Table 3: Results of the statistical investigations, illustrated here as correlation matrix values.